ARMY RESEARCH LABORATORY

Haltere Mechanics and Mechanical Logic for Micro-Electro-Mechanical Systems (MEMS) Scale Bio-inspired Navigation Sensors (Final Report)

by Gabriel Smith, Sarah Bedair, Brian Schuster, and William Nothwang

ARL-MR-0807   **February 2012**

NOTICES

Disclaimers

The findings in this report are not to be construed as an official Department of the Army position unless so designated by other authorized documents.

Citation of manufacturer's or trade names does not constitute an official endorsement or approval of the use thereof.

Destroy this report when it is no longer needed. Do not return it to the originator.

Army Research Laboratory

Adelphi, MD 20783-1197

ARL-MR-0807   **February 2012**

Haltere Mechanics and Mechanical Logic for Micro-Electro-Mechanical Systems (MEMS) Scale Bio-inspired Navigation Sensors (Final Report)

Gabriel Smith, Sarah Bedair, and William Nothwang
Sensors and Electron Devices Directorate, ARL

Brian Schuster
Weapons and Materials Research Directorate, ARL

REPORT DOCUMENTATION PAGE

1. REPORT DATE *(DD-MM-YYYY)*	2. REPORT TYPE	3. DATES COVERED (From - To)
February 2012	DRI	FY11

4. TITLE AND SUBTITLE	5a. CONTRACT NUMBER
Haltere Mechanics and Mechanical Logic for Micro-Electro-Mechanical Systems (MEMS) Scale Bio-inspired Navigation Sensors (Final Report)	
	5b. GRANT NUMBER
	5c. PROGRAM ELEMENT NUMBER

6. AUTHOR(S)	5d. PROJECT NUMBER
Gabriel Smith, Sarah Bedair, Brian Schuster, and William Nothwang	FY11-SER 044
	5e. TASK NUMBER
	5f. WORK UNIT NUMBER

7. PERFORMING ORGANIZATION NAME(S) AND ADDRESS(ES)	8. PERFORMING ORGANIZATION REPORT NUMBER
U.S. Army Research Laboratory ATTN: RDRL-SER-L 2800 Powder Mill Road Adelphi, MD 20783-1197	ARL-MR-0807

9. SPONSORING/MONITORING AGENCY NAME(S) AND ADDRESS(ES)	10. SPONSOR/MONITOR'S ACRONYM(S)
	11. SPONSOR/MONITOR'S REPORT NUMBER(S)

12. DISTRIBUTION/AVAILABILITY STATEMENT

Approved for public release; distribution unlimited.

13. SUPPLEMENTARY NOTES

14. ABSTRACT

Small autonomous aerial systems require the ability to detect roll, pitch, and yaw to enable stable flight. Existing inertial measurement units (IMUs) are incapable of accurately measuring roll-pitch-yaw within the size, weight, and power requirements of small autonomous systems. To overcome this, we have designed novel IMUs based on the biological haltere system in a microelectromechanical system (MEMS). MEMS haltere sensors were successfully simulated, designed, and fabricated with a control scheme that enables simple, straightforward decoupling of the signals. Passive mechanical logic was designed to facilitate the decoupling of the forces acting on the sensor. The control scheme was developed that efficiently and accurately decouples the three component parts from the haltere sensors. Individual, coupled, and arrayed halteres were fabricated. A series of static electrical tests and dynamic device tests were conducted, in addition to in-situ bend tests, to validate the simulation results, and these, taken as a whole, indicate that the MEMS haltere sensors will be inherently sensitive to the Coriolis forces caused by changes in angular rate. The successful fabrication of a micro-angular rate sensor represents a substantial breakthrough and is an enabling technology for a number of Army applications, including micro air vehicles (MAVs).

15. SUBJECT TERMS

Angular rate sensor, ARS, haltere, MEMS

16. SECURITY CLASSIFICATION OF:			17. LIMITATION OF ABSTRACT	18. NUMBER OF PAGES	19a. NAME OF RESPONSIBLE PERSON
a. REPORT	**b. ABSTRACT**	**c. THIS PAGE**	UU	38	Gabriel Smith
Unclassified	Unclassified	Unclassified			**19b. TELEPHONE NUMBER** *(Include area code)* (301) 394-3722

Contents

List of Figures

List of Tables

Acknowledgments

1. Objective

Small autonomous systems require a series of navigational sensors to achieve autonomy. One of the most critical sensor modalities to a flying robot is the ability to detect roll, pitch, and yaw. Inertial measurement units (IMUs) that are capable of measuring roll-pitch-yaw for large scale platforms exist; however, these devices are large, power hungry, require vacuum packaging, and fundamentally fail at the smaller sizes as they would cripple the entire mobile microsystem. Coupling the capability developed under this Directors Research Initiative (DRI) with existing technology for optical flow would enable navigation beyond what navigation grade IMUs are currently capable of. Current drive motors typically couple large amounts of energy into the IMUs, and these effects tend to become exacerbated at smaller scales, making existing IMUs ineffective.

It is therefore necessary to design a new IMU mode that is not susceptible to the system noise but is still sensitive enough to accurately measure the system roll-pitch-yaw. Biologically, insects achieve this by utilizing two halteres, which are weighted pendulums that oscillate. The two halteres have a series of hair-like sensors around the base of the pendulum (sinsilla) that detect the out-of-plane motion caused by roll-pitch-yaw induced Coriolis forces. It had long been thought that halteres were passively driven to oscillate; however, this is not the case. They are actively driven by the flight muscles, which also accounts for the matched frequency but out of phase nature of the oscillations (Pringle, 1948).

Mechanical halteres have been previously investigated for flying platforms of this scale (Wu et al., 2003; Chen et al., 2007). They have demonstrated that Coriolis effects are measureable with these devices. Most research to date, though, has focused on a passively driven, single (i.e., non-coupled) haltere. While Coriolis effects are indeed measureable with this type of device, they are still sensitive to system noise, and they require a significant amount of computation to decouple the various components of the force equation. By driving the haltere at an optimum frequency, it should be possible to minimize the system noise effects, and by coupling two halteres, it should be possible to differentially sense the roll-pitch-yaw and substantially simplify the force equation.

The objectives for this research were the following:

1. Apply the force equations to uncoupled and coupled halteres. (*2Q, Accomplished*)

2. Use the results of the theoretical investigation to determine the optimal size, materials and drive frequency of the halteres in both coupled and uncoupled states. (*2Q, Accomplished*)

3. Fabricate a microelectromechanical system (MEMS)-scale haltere. (*3Q, Accomplished*)

1

4. Test and characterize the performance of the MEMS-scale haltere, and compare the results to the theoretical predictions. (*4Q, Partially Accomplished*)

To date, concept generation, advanced modeling, and fabrication on the angular rate sensor has been completed and is reported here. *At time of submission (December 2011), the size of the sensor system, to be developed within this DRI is the world's smallest angular rate sensor.*

2. Approach

Proprioceptive sensors enable mobility control for mm-scale robotics and are essential to achieving stable flight in aerial autonomous systems, but they are challenging to integrate at this scale. For instance, stable hover of the aforementioned mm-scale flapping wing platforms requires three types of proprioceptive control. These include a means of orientation control, three-axis relative velocity control, and three-axis angular rate control. Examining biology, most flying insects, particularly two wing or order diptera, use both visual and inertial sensors for stable flight (Wu et al., 2003). Research has shown that diptera use visual cues and optic flow for orientation and velocity data. They sense angular rate through a Coriolis force measurement on a vibrating club-like structure call a haltere. Sherman and Dickinson found both the compound eyes and the mechanosensory halteres encode angular motion as the fly rotates about the three body axes during flight. The visual system is tuned to relatively slow rotation whereas the haltere-mediated response to mechanical rotation increases with rising angular velocity (Sherman and Dickinson, 2003).

Traditional, packaged rate sensors do not possess compatible size, weight, and power (SWaP) to be practical for mm-scale autonomous systems (Wu et al., 2003). The mass of current state-of-the-art vibrating MEMS angular rate sensors is individually larger than the desired target mass of expected entire robotic systems, requiring alternative integration strategies. One integration option would be to eliminate the lead frames and plastic encapsulation then die bond the sensor directly to the robot. Non-traditional packaging, sensor die integration, and sensor protection creates many difficult engineering issues at this scale. This is possible but entails packaging size and weight trade-offs. Ideally, the rate sensors would be monolithically integrated in the robotic platform fabrication process and would also operate effectively in air, eliminating the need for vacuum packaging. Wu et al. demonstrated a bio-mimetic, angular rate sensor (ARS) that can detect angular rates of 1 rad/s and are 5-mm in length driven by bulk lead zirconate titanate (PZT) actuators (Wu et al., 2003). However, these are not small enough to integrate directly with many micro air vehicles (MAVs).

The halteres in insects, shown in figure 1, measure the resultant Coriolis forces (caused by the angular rates) and motion orthogonal to the direction of haltere oscillations. Force sensing hairs are connected to their neural system at the base of the haltere. Inspired by the insect sensors, a

MEMS-based pendulum structure that is both actuated and sensed using the piezoelectric effect has been fabricated. The MEMS ARS are designed to be capable of being monolithically integrated with piezoelectric mobility actuators, thus enabling direct proprioceptive control of mm-scale and cm-scale robotic platforms. The U.S. Army Research Laboratory (ARL) piezoelectric MEMS (PiezoMEMS) ARS (figure 2) maximizes the sensitivity to rotational rate (roll-pitch or yaw) for a minimal SWaP requirement.
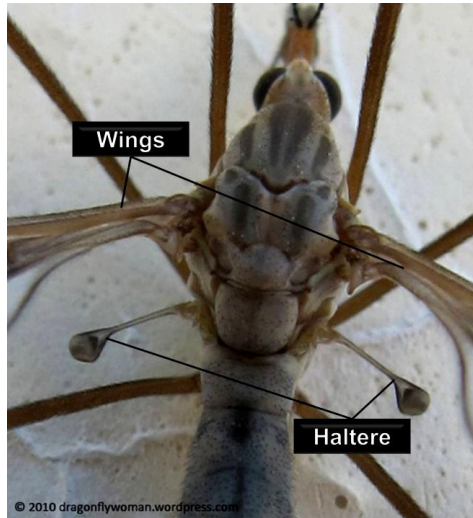
Figure 1. Example of the club-like haltere location (circled) relative to the wings of diptera on a giant crane fly (Woman, 2010). The haltere is believed to be a devolved hind wing as four-wing insects do not have this structure. Two haltere can give information on all three axes of rotation.
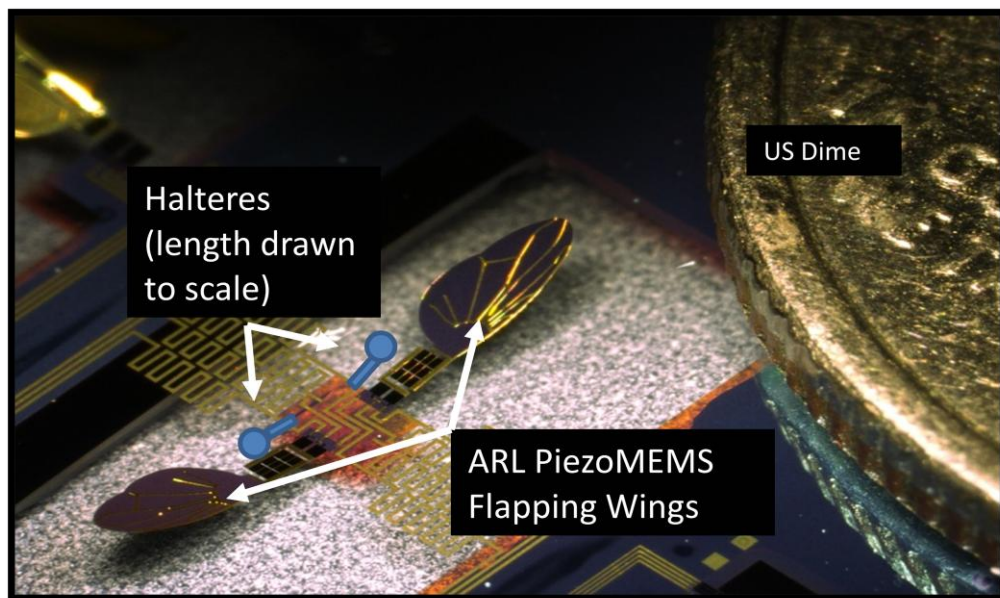
Figure 2. Illustrates concept of integrating Piezo MEMS haltere with the ARL PiezoMEMS flapping wing. In this conceptual drawing, 500-μm halteres are drawn to scale relative to the wings.

PZT actuators can be used for mobility in small robotic systems. Alternatively, the voltage generated by applied stresses in the PZT can be used for inertial sensing. This report details the design, fabrication, and preliminary results of a biologically inspired, low-power, two-axis ARS to be integrated into micro-robotic aerial platforms.

There were three distinct portions of this research. First, a fundamental mechanics analysis and systematic scaling investigation was completed. The results of the fundamental mechanics are reported elsewhere (Jordan et al., in preparation). In this report, the set of passive mechanical logic developed as a result of this analysis is presented, covering the other two parts of this research, namely, an examination of analog circuit development suitable for the control and the development, fabrication, and testing of a MEMS-scale, haltere-based ARS system.

2.1 Fundamental Mechanics Analysis

To fabricate an engineered ARS system based upon the biological haltere system, it was first necessary to understand to the degree possible how biological systems use haltere campaniform sensors and process the data. To a large extent, biological systems that utilize haltere input have been well studied, beginning with the work of Pringle (Frankel and Pringle, 1938). Within the scope of the DRI, we examined the biological system studies (Pringle, 1948; Thompson, 2009; Thompson et al., 2009; Motamed and Yan, 2005; Alexander, 2007; Bender and Frye, 2009) and the developed engineering analogs, where appropriate. These engineering analogs focused on (1) control electronics for haltere sensors and (2) physics-based, engineering design models. Once a thorough understanding of the biological system was completed and physics-based engineering design models were accomplished, it was possible to develop scaling models that would enable fabrication and design of a MEMS-scale haltere-based sensor system.

The Coriolis term is proportional to the cross product of the angular velocity of the frame and instantaneous haltere velocity, and it is generally found to be several orders of magnitude greater than the angular acceleration of the mass and several orders of magnitude smaller than the centripetal acceleration (Wu et al., 2002). Summing the moments with damping, stiffness, and inertial forces around the base of the haltere gives the following equation of motion:

$$
\begin{aligned}
\ddot{\theta} + 2\zeta\omega_n\dot{\theta} + \omega_n^2\theta ={}& \dot{\Omega}_3\sin(\gamma) - \dot{\Omega}_1\cos(\gamma) - \dot{\gamma}^2\cos(\theta)\sin(\theta) \\
& + 2\dot{\gamma}[(\Omega_3\cos(\gamma) + \Omega_1\sin(\gamma))\cos^2(\theta) \quad - \Omega_2\cos(\theta)\sin(\theta)] \\
& + (\Omega_3^2\cos^2(\gamma) + \Omega_1^2\sin^2(\gamma) - \Omega_2^2)\cos(\theta)\sin(\theta) \\
& + (\Omega_2\Omega_3\cos(\gamma) + \Omega_1\Omega_2\sin(\gamma))\cos(2\theta) + 2\Omega_1\Omega_3\cos(\theta)\sin(\theta)\cos(\gamma)\sin(\gamma)
\end{aligned}
$$

(1)

In equation 1, ζ is the damping factor of the system, ω_n is the natural frequency, γ is the angular position of the haltere, and θ is the angle of displacement. Ω_1, Ω_2, and Ω_3 are the angular velocity components (roll, pitch, and yaw) of $\hat{b}_1$, $\hat{b}_2$, and $\hat{b}_3$ axes, respectively. Ω_1 and Ω_3 are the in-plane body rate components with respect to the $\hat{b}$-axis, and Ω_2 is the out of plane body rate component with respect to the $\hat{b}$-axis.

In biological systems, Pringle's analysis indicated the scale on which haltere can be implemented with the payload only amassing to about 20 µg (0.08% of total weight) in a *C. erythrocephala* system (Pringle, 1948). If an engineered system based on the haltere could be implemented, there are substantial power and weight savings as well as improved sensitivity that could be realized. To accomplish this, however, it is necessary to first solve the complex force decoupling problem shown in equation 1 without a loss of sensitivity.

To fully implement a haltere-based ARS system, it is necessary to fully decouple the multiple forces acting on an individual haltere. Additionally, it is critical to isolate the haltere signals from any system vibration that may couple into the vibrating pendulum. Figure 3 shows the general frame of reference and the complex interactions of the multiple forces that are acting on the halteres.
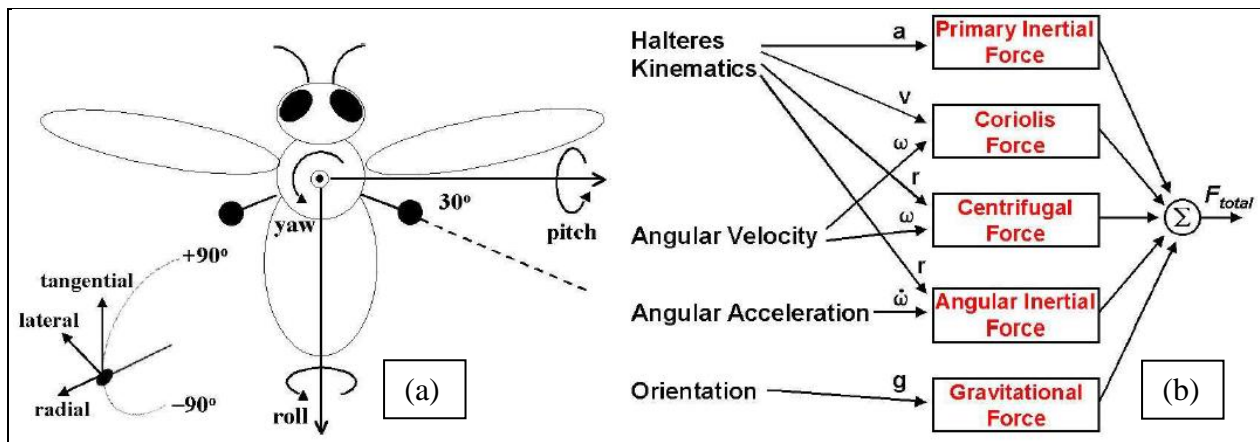
Figure 3. (a) A schematic showing the halteres and the roll, pitch, and yaw axes and (b) indicates all of the different forces that are acting upon the halteres (Wu et al., 2003).

Employing these fundamental mechanics of the system, it was possible to design a passively filtering mechanical system to simplify the signal demodulation. The details of this are addressed in section 3.

The full details of the biomechanics review can be found in an ARL technical report (Jordan et al., in preparation) that is being prepared for publication. The synopsized version has been presented here.

2.2 Analog Circuit Design and Control Methodologies

The fundamental physics-based models that are described earlier were used to develop simplified circuits capable of detecting, amplifying, and decoupling the three component angular rate vectors. In order to determine the angular rotation of a flying robot using mechanical haltere, the roll, pitch, and yaw must be pulled from the left and right haltere signals. By coupling the beat frequency of the wings to the haltere input, it is possible to demodulate the coupled signal to determine the roll, pitch, and yaw of a flying robot, and isolate each signal by appropriate signal

demodulation. Each component angular rate can then be calculated directly from these signals by amplifying them with a gain of $-1/2m$, where m is the mass of the haltere since the Coriolis force is expressed by $2m\omega \times v$.

2.3 MEMS-scale Device Design, Fabrication and Testing

This section details the design, fabrication, and testing of a biologically inspired, low-power, two-axis ARS to be integrated into micro-robotic aerial platforms. Thin-film PZT sensors will enable a reduction in the order of magnitude in haltere length with similar sensitivity. The ability to convert strain in the film to a voltage can be used as an inertial sensor. Furthermore, the PZT-based haltere can also drive itself into resonance by using areas of the PZT as out-of-plane bending actuators (Wu et al., 2003).

Modeling and testing indicates a system that is inherently sensitive to the Coriolis forces caused by changes in angular rate. Scale studies and modal analysis were completed to guide the MEMS-level sensor development. MEMS-based halteres have been fabricated as individual die and in coupled arrays. Understanding the coupling mechanisms between multiple halteres will enable triaxial-sensitivity at lower SWaP and thus will contribute to unmanned aerial vehicles at an unprecedented scale.

MEMS-based haltere sensors were designed and simulated in ANSYS. The MEMS-based halteres were fabricated in the ARL Specialty Electronic Materials and Sensors Cleanroom (SEMASC) through a PZT/copper (Cu) process that was developed in a concurrent DRI (Bedair et al., 2012) and is described elsewhere. Details from both the fabrication and simulations are given in section 3.

2.4 Mechanical/Materials Properties of the Complex Heterostructure

The surface morphologies, microstructures, and layer thicknesses of the fabricated halteres' complex heterostructure were examined in an FEI Nano600i dual beam focused ion beam (FIB) and scanning electron microscope (SEM). This instrument has coincident ion and electron columns that allow for site-specific micro-machining and high resolution imaging. The quasi-static mechanical response of the structures was investigated with a custom in situ SEM mechanical test stage. The stage features a three-axis piezoelectric stage that allows specimen manipulation over a 5-mm range with step resolution approaching 100 nm. Loads were applied using a direct drive piezoelectric linear actuator with reported sub-nanometer resolution and were measured by a strain gage based S-beam load cell (capacity of 100 g and resolution of ~0.01 g or 0.1 mN). In this work, a tungsten needle flattened using FIB machining and this was used for load application.

3. Results

MEMS-scale haltere sensors were successfully designed and fabricated with a control scheme that enables simple, straightforward decoupling of the signals. There are three principal successes that enabled that and they are presented in this section. First, passive mechanical logic was designed to facilitate the decoupling of the forces acting on the sensor; second, an analog circuit design was developed that efficiently and accurately decouples the three component parts from the haltere sensors; and third, individual, coupled, and arrayed halteres were fabricated in the MEMS foundry at ARL's Adelphi Laboratory Center (ALC). In an effort to facilitate the long-term optimization of these sensors, the materials, composite, and dynamic testing has been initiated and is underway on the completed sensors.

3.1   Passive Mechanical Logic

Mechanical logic typically refers to the implementation of Boolean logic functions in mechanical parts, such as the single pole double throw relay and the 3-bit, piezoelectric MEMs analog-to-digital (A-D) converter described by Proie et al., (Proie et al., 2011). This type of logic, which can be integrated with standard complementary metal-oxide semiconductor (CMOS) logic and is capable of performing many of the same calculations and controls that traditional CMOS accomplishes, can also directly integrated with the haltere sensors and the MAV, as shown in figure 2. Proie et al. are using this mechanical logic to construct an extremely low power microcontroller. The development of this topic is well covered elsewhere (Smith et al., 2011; Proie et al., 2011) and is not be directly discussed here. However, in addition to the active mechanical logic, it is possible to take advantage of the inherent passive mechanical and materials properties of a structure to selectively filter, modulate, and combine different signals. Passive filtering and signal sampling were both exploited in the development of the haltere sensors.

To fully decouple the individual forces acting on a haltere, it is necessary to reexamine equation 1. To accomplish a reduction in complexity without any loss of accuracy, one modulates a haltere signal with the beat frequency. Taking a closer look at equation 1, the inherent mechanical nature of the individual, and coupled, haltere can be exploited. If we sample the signal when the halteres are near 0 and π, all of the sine terms in equation 2 go to zero. Similarly, at $3\pi/2$ and $\pi/2$ all of the cosine terms are zero. The cross terms are zero at both. Similarly, the sign of the input will be positive for the left haltere for Ω_{roll}, when it is negative for the right. Ω_{pitch}, however, is always the same sign for left and right. Ω_{yaw} has opposite sign from left to right and twice the frequency as Ω_{roll}. The individual haltere signals for each Ω are shown in figure 4. As such, it is possible to utilize the inherent frequency response for each of the signals to isolate Ω_{roll}, Ω_{pitch}, and Ω_{yaw} by simply selectively adding and subtracting the signals from the frequency modulated right and left haltere. The force in the roll direction is modulated

with the beat frequency in the left haltere and with the beat frequency with a 180° phase shift for the right haltere. The force in the pitch direction is modulated with the beat frequency with a 180° phase shift for both halteres. The force in the yaw direction is modulated with twice the beat frequency in the left haltere and with twice the beat frequency with a 180° phase shift for the right haltere. These signals are added together to produce the overall force on each haltere.
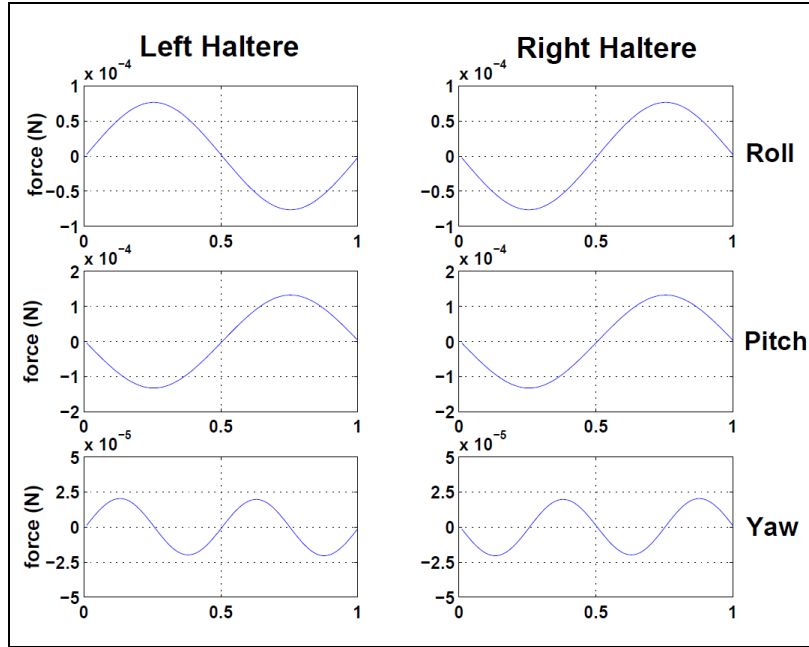
Figure 4. Modulation of three signals over a single haltere cycle.

The second principal obstacle to designing a haltere-based ARS is the susceptibility of oscillating systems to coupling external vibrations into the inherent oscillations of ARS. There are two mechanical solutions to this problem that have been employed within this project, mechanical filtering and frequency selection.

Mechanical filtering takes advantage of a motional impedance mismatch that exists between adjacent portions of a structure. Figure 5 shows a schematic of a haltere where the PZT drive beam is in the *xy* plane and is connected to the high aspect ratio beam that is in the *xz* plane. At this contact, there will be a high motional transfer impedance due to the geometrical anisotropy, and most vibrational energy will be reflected back into the *xy* plane and not transferred to the *xz* plane. While some energy will be transferred due to the Poisson coupling, this is a relatively small amount.
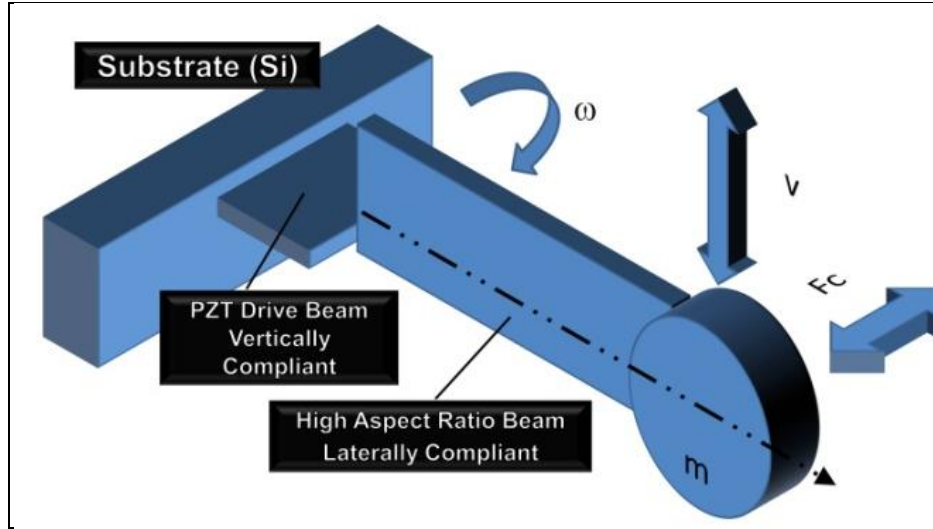
Figure 5. Vectors show orthogonal velocity (v) and Coriolis forces (F_c) on a mass due to angular rate (ω) about the illustrated axis vectors on a notional haltere. The orthogonal aspect ratios of the beam allow for compliance in the drive and sense direction.

In our MEMS haltere design, we fabricate a three-dimensional (3-D) MEMS structure with a thin cantilever in the *xy* plane connected to the structure at one end and the pendulum mass in the *xz* plane at the other. The pendulum mass is substantially thicker in the *z* direction than the cantilever. This will substantially increase the transfer impedance from the structure to the pendulum mass and isolate the sensor from much of the structure vibrational noise. A careful understanding of modal frequencies and shapes must also be employed to accomplish this. This is further discussed in sections 3.3 and 3.4.

It is important to note that this method to reduce system noise only addresses vibrations within the frame and does not address vibrations of the frame. In flapping wing flight, in particular, the entire super-structure will heave with each flap of the wing. Additionally, MAVs are susceptible to flight noise. The halteres will detect both of these signals. Methods to detect and decouple flight noise are not directly addressed in this report. However, to address the issues of heave, it is possible to passively filter the signal by applying frequency selection. The wings will create a substantial heave motion with each stroke that has components of all three angular accelerations. Each component has a frequency dependence associated with the overall flap frequency that can couple into the haltere and generate erroneous signals. Biologically, insects use the same frequency for the flap and the haltere, and this is a viable method to modulate the haltere signal and wings as this will create a coupled response.

Alternatively, it is possible to isolate the haltere from the wings by selecting a $f_{haltere} \neq f_{wings}$. So long as $f_{haltere}$ is not an integer factor of f_{wings}, it is possible to average over many haltere cycles to remove the spurious signal associated with the wings. This method improves signal to noise but will has a slower response time and is susceptible to oversimplifying the signal. While in the initial designs $f_{haltere}$ is ~500 Hz and is substantially different than f_{wings}, and this would enable

9

the implementations of an averaged sensor scheme, the eventual haltere design will likely utilize $f_{haltere} = f_{wings}$. The initial beat frequency of the halteres was chosen as a design point around which the other mechanical properties of the halteres could be optimized, as it is relatively straightforward to design for operation at a specific frequency once the device has been optimized.

3.2   Demodulation Circuit Design

The fundamental physics-based models that are described earlier were used to develop simplified circuits capable of detecting, amplifying, and decoupling the three component angular rate vectors. In order to determine the angular rotation of a flying robot using mechanical haltere, the roll, pitch, and yaw must be pulled from the left and right haltere signals. The force signal in each direction of rotation is modulated based on the beat frequency of the haltere and added to the modulated force in the other two directions to yield the total force on a haltere. The three signals are modulated over a single haltere cycle according to figures 3 and 4.

The force in the roll direction is modulated with the beat frequency in the left haltere and with the beat frequency with a 180° phase shift for the right haltere. The force in the pitch direction is modulated with the beat frequency with a 180° phase shift for both haltere. The force in the yaw direction is modulated with twice the beat frequency in the left haltere and with twice the beat frequency with a 180° phase shift for the right haltere. These signals are added together to produce the overall force on each haltere. To determine the roll, pitch, and yaw of a flying robot, these signals are separated according to the following scheme in figure 6.
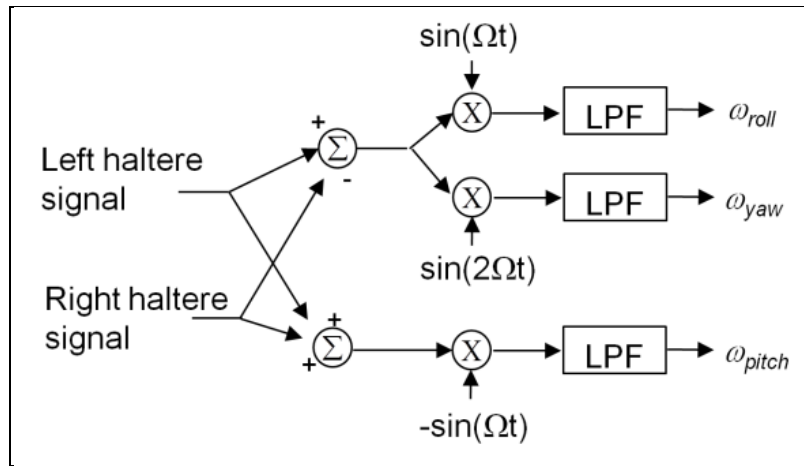
Figure 6. Signal separation scheme (Wu et al., 2003).

The full circuit built and tested is shown in figure 7. To decouple the signals in which the force on the left haltere is in and out of phase with the force on the right haltere, summing and differential circuits are implemented. If the right haltere signal is subtracted from the left haltere signal, the resulting signal consists of only roll and yaw because the in-phase pitch signals will cancel each other. If the signals from the two halteres are added together, only the pitch signal

will remain because the anti-phase signals will cancel each other out. Next, the signals are demodulated. The roll and yaw signal is first demodulated by the beat frequency in order to produce roll. The same signal is also demodulated by twice the beat frequency to yield yaw. The pitch signal is demodulated by the beat frequency with a 180° phase shift. These three signals are then passed through low pass filters, each with a cut-off frequency of 100 Hz.
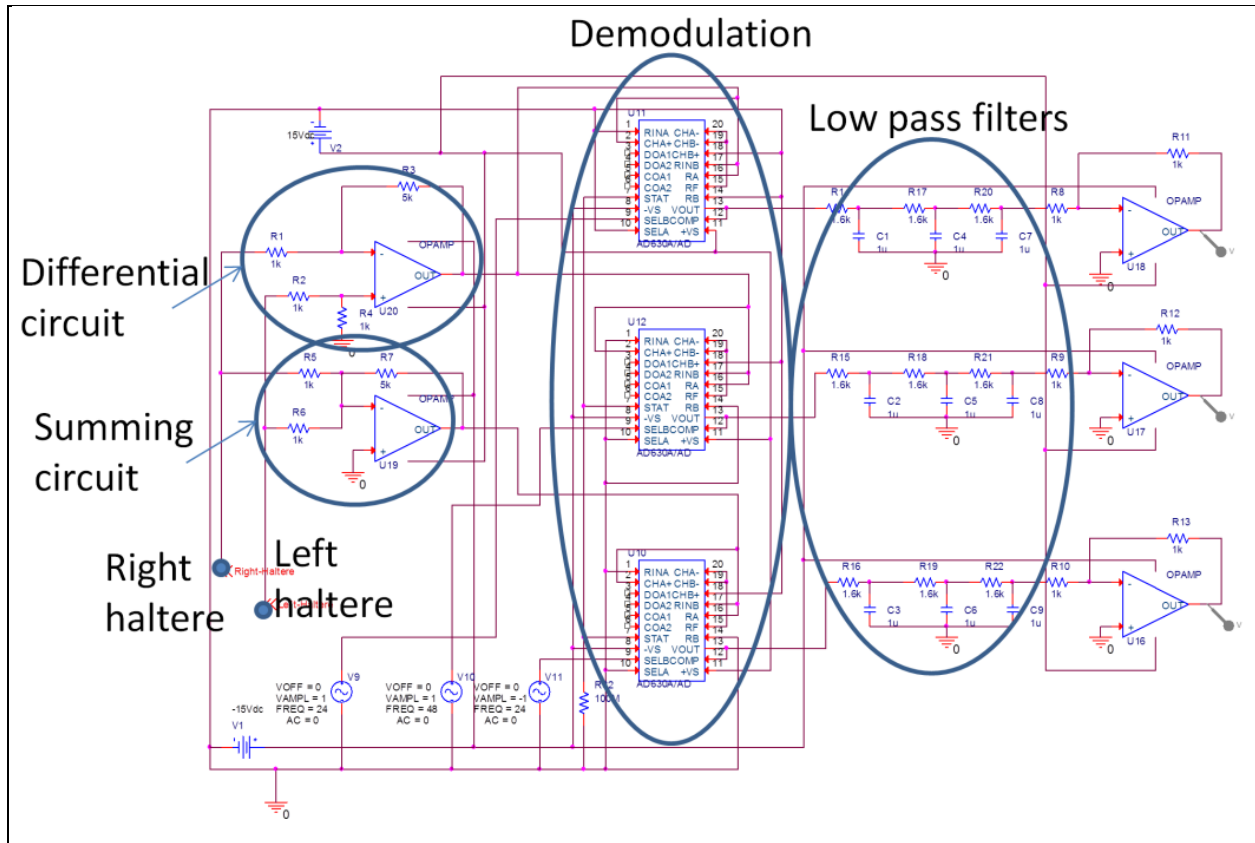
Figure 7. Complete haltere demodulation, filtering and amplification circuit to yielding three independent, angular rates.

Once the complete circuit was designed and built, a series of three simulations were performed to validate the design. Custom LabVIEW programs were created to drive the experimental setup, as described below. For a complete description of the LabVIEW experimental programs associated with this research, please consult the companion ARL technical report (Jordan et al., in preparation). Following are graphs of the demodulated signal; these are the outputs of the circuit designed and built in figure 7. The three signals represent simulated roll, pitch, and yaw. Figure 8 shows these three coupled signals overlaid after they have been demodulated (note that these are simulated signals from a function generator).
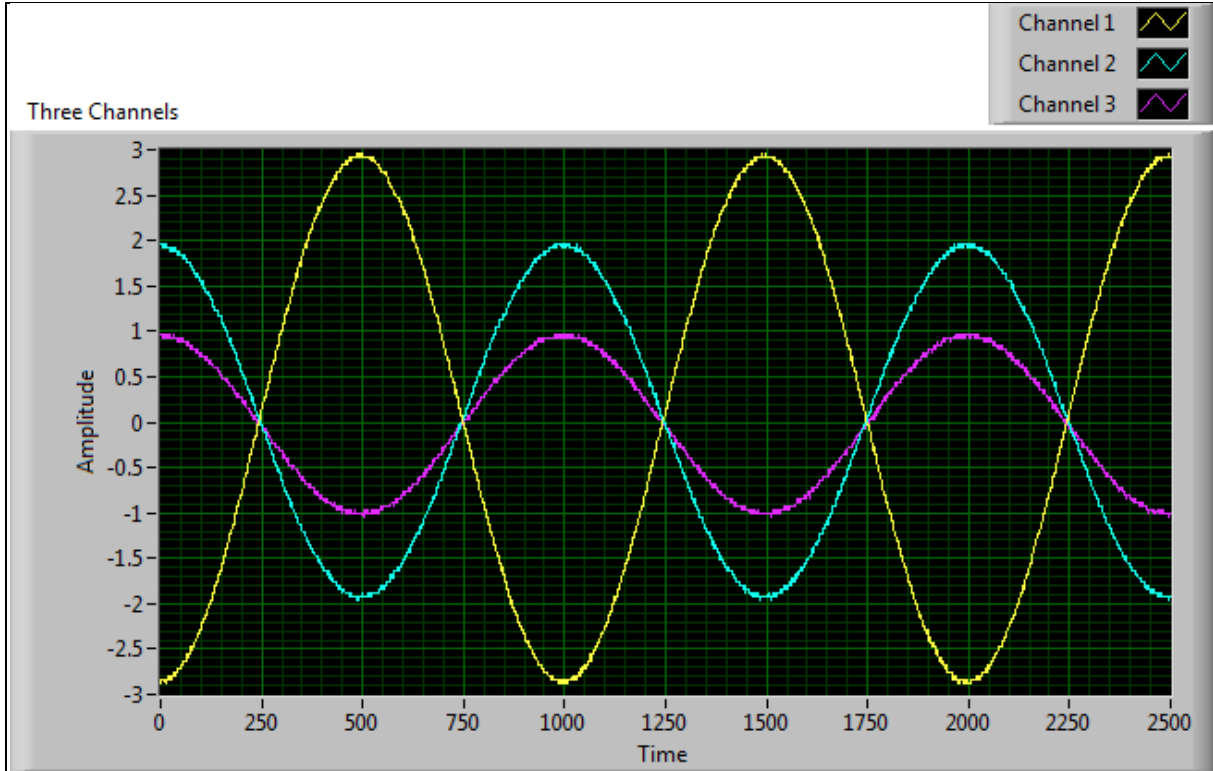
Figure 8. Results of the simulation experiments with a complete haltere signal demodulation and amplification using the designed Circuit to yield three independent, angular rates. Channel 1 represents roll, channel 2 is pitch, and channel 3 is yaw.

3.3 MEMS-scale Device Design, Fabrication and Testing

For a MEMS-based haltere, figure 5 illustrates the general concept with the Coriolis forces (F_c) acting on the end mass due to angular rate about the illustrated axis vectors. The MEMS-scale design was built upon the findings of the fundamental analysis that was described earlier. First simulations of the design space were conducted in ANSYS. Second, a process flow was developed to enable the incorporation of the PZT thin films with the Cu plating process developed by Bedair et al. (2012). Finally, a series of three wafer runs were conducted, each building upon the findings of the previous run, to fabricated MEMS-scale halteres.

3.4 Analytical and Numerical Modeling

During the simulations, there were a number of very important aspects of the device design that were investigated. To ensure that the concept described in figure 11 would be valid for dimensions available in the fabrication process, modal analysis in ANSYS was performed. Parametric studies across the range of reasonable low fabrication risk minimum and maximum dimensions increase the chance the MEMS halteres will function with high yield as intended on the first release. Modal analysis is also essential for two other important reasons. First, the frequencies and mode shapes were extracted and the design was chosen so that the second sensing mode is sufficiently higher in frequency than the drive mode. This means the orthogonal

sensing will respond to the frequency but not in a resonant mode. Also knowing the fundamental mechanical frequency of a haltere structure allows the investigators to match the frequency of the flapping wing if it the haltere is driven passively by the system instead of actively.

The second reason is ANSYS can compare the respective relative stresses in the beams and make sure they are concentrated in such a way to avoid interfering with the piezoelectric sensing signal (figures 9 and 10). Ultimately, the electrical, mechanical, materials and piezoelectric properties of the different layer of the complex heterostructures that would become the haltere sensors were optimized to generate the maximum sensor output for a given Coriolis force input, while minimizing the signal noise due to coupling between the sense axis and the pendulum swing axis. To achieve this, the dimensions and materials were chosen to concentrate the stress associated with the pendulum motion in a different portion of the cantilever than the stresses associated with the Coriolis forces. Material coupling was then optimized such that the piezoelectric PZT sensors at the base of the cantilever were able to detect the Coriolis force impinging force at the tip of the cantilever. It is also important to have the center of mass as far from the base of the cantilever as possible to maximize the sensitivity, and for this reason, it was decided to use the Cu plating process instead of a traditional silicon (Si) mass at the tip. Cu has a density that is 3.8 times that of Si so for the same rotation rate and drive frequency a Cu mass of the same volume experiences 3.8 times the Coriolis force. This ultimately reduces the footprint and therefore cost of the sensor.
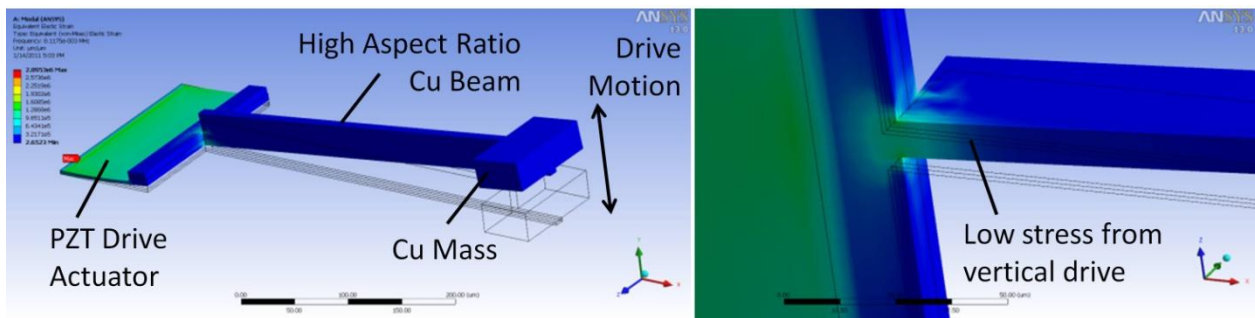

Figure 9. ANSYS modal analysis showing drive or actuation mode shape, out of plane motion and relative strain at the root of the high aspect ratio beam due to the drive motion.
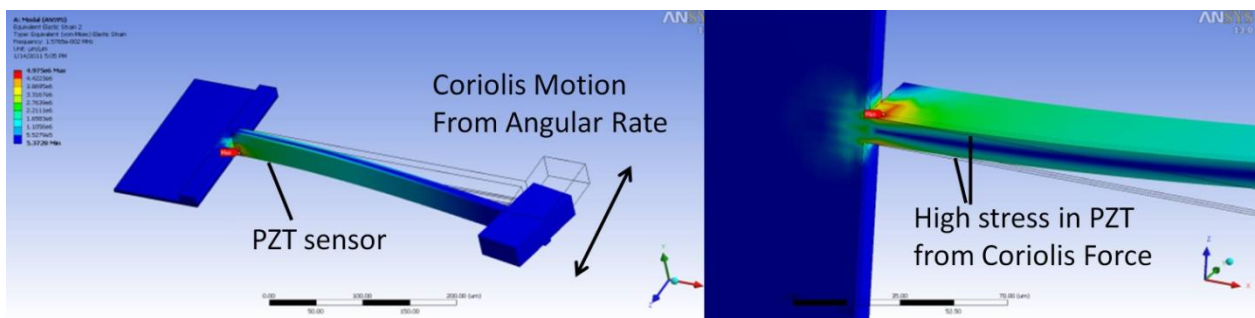

Figure 10. ANSYS modal analysis showing the Coriolis force sensing mode shape, in-plane motion and relative strain along the sides of the high aspect ratio beam due to the sideways motion.

Figure 9 and 10 show an example of the ANSYS modeling used to predict and optimize the mode shape and natural frequencies of the drive and sense modes shapes, respectively. The halteres are designed so the natural frequency of the sense mode shape is at least two to three times higher than the drive frequency. This is to ensure the haltere sensors can respond to the frequency of the Coriolis force.

In addition to the ANSYS modeling, an analytical model was developed to vet the various designs. Equation 2 shows the final result of the analytical model used to determine if the PZT available could generate a minimum detectable voltage at an angular rate of 1 rad/s. A rate of 1 rad/s was chosen as the sensitivity of the haltere in (Wu, 2003) with an order of magnitude in size reduction. Iterative optimization of this MEMS design should demonstrate greater sensitivity. Figure 11 shows a MATLAB simulation to optimize the copper mass loading to the end of the cantilever.
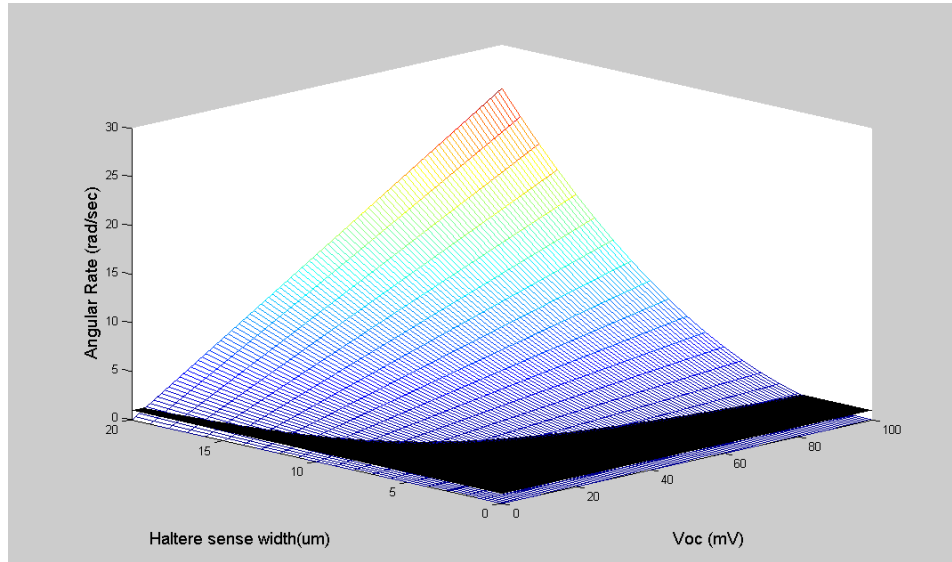
Figure 11. Example of a MATLAB run testing the effect of changing Cu beam width to angular rate and minimum detectable output voltage.

$$\omega_{\min}(V_{oc}) = \frac{t_{Cu}w_{Cu}{}^{2}\varepsilon_{o}\varepsilon_{33}A_{total}Y_{Cu}V_{oc\min}}{12\pi L_{m}w_{m}t_{m}\rho_{Cu}L_{h}{}^{2}f\,\sin\!\left(\dfrac{\theta}{2}\right)A_{PZT}d_{31}Y_{PZT}t_{PZT}} \tag{2}$$

The sense PZT electrodes are placed in such a way to experience the maximum strain when the beam bends in the plane of the wafer. They sit on an oxide layer (figure 10) along either side of the high aspect ratio Cu beam. This is the areas of stress concentration shown in figure 10. Ideally, to maximize signal, they would "coat" the side walls of the Cu beam, but no process exists to do so. This configuration is a compromise but fabricated well. The PZT was stopped at the intersection of the two beams. The gold (Au) traces running to the sensors pick up the signal

and pull it down the drive beam. This was done to eliminate the PZT signal on the active bending drive beam.

As described earlier, insects use two halteres to extract three-axis rotational motion components. By swinging the haltere in a 180° arc out of plane, each haltere sweeps through two axes. One axis changes sign throughout the stroke; therefore, the frequency of the signal is twice that of the other axis. A robotic integrated haltere can mimic this sensor. The state of the art of the MEMS process at ARL has made MEMS wings that sweep through a similar arc of up to 145°. This should allow for two halteres to gain information on rotations in three directions. Furthermore the fabrication process easily makes orthogonal haltere in plane (roll and pitch) but the yaw axis is out of the plane. By intending to swing the halteres into the yaw axis, fabrication and packaging of the three-axis system becomes simpler.

3.5   Device Fabrication

The process used to fabricate these devices is similar to the process used in ARL to fabricate PiezoMEMS RF switches, resonators, and the ARL mm-scale flapping wings (Smith et al., 2011). A key distinction is the addition of three Cu layers in the process. The integration of the PiezoMEMS and the Cu layers was developed and demonstrated for the first time in a concurrent FY11 DRI (Bedair et al., 2012) to make PiezoMEMS tunable inductors. The haltere test devices were made in the same process on the same wafers. Leveraging the two DRI efforts was a key component to the success of this project as the high aspect ratio Cu beams were integrated with higher yield than in previous attempts with Si.

All fabrication was performed in the ALC cleanroom. The process cross section is shown in figure 12. The PZT thickness was targeted at 1 micron and the Cu layers are nominally 10 microns each. Other layers are shown in more details of the fabrication processes can be found in the other FY11 DRI (Bedair et al., 2012). Table 1 shows relative thicknesses for a haltere heterostructures. In figure 13 a graphical cross-sectional representation of the devices is given, and it is possible to visualize the substantial thickness differences that were achieved using the novel Cu plating process developed by Bedair and Meyer. In figure 14, actual fabricated haltere are shown. The thicknesses of the copper layer were designed to increase in devices from left to right. This will allow evaluation of the optimal thickness as a function of cantilever length.
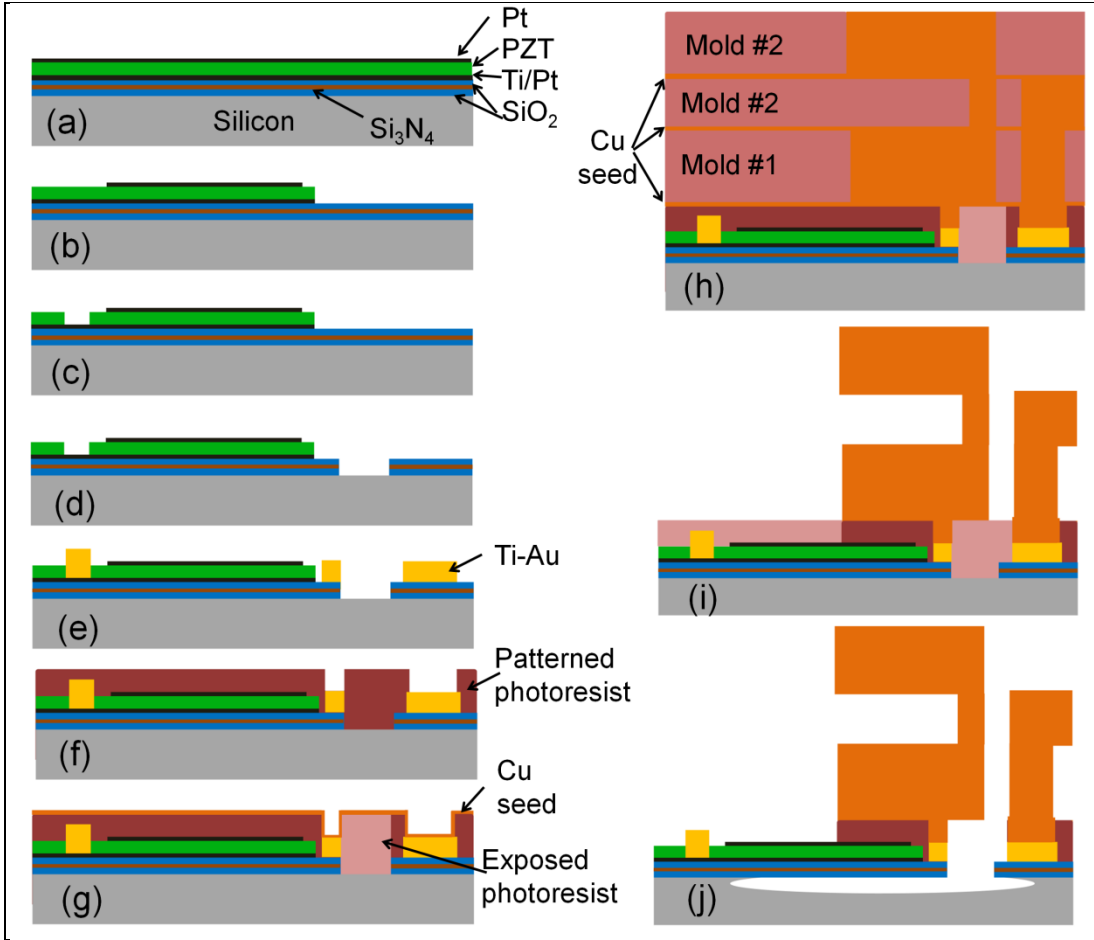
Figure 12. ARL PZT/Cu process flow cross section developed by Bedair and Meyer. (Bedair et al., 2012).

Table 1. Representative thicknesses for each layer of the complex PZT-Cu-silicon dioxide (SiO$_2$) structure.

| Material	Nominal Thickness
Cu	10–30 μm
Top Pt	1000A
PZT	1 μm
Bottom Pt	1000A
SiO$_2$	2 μm
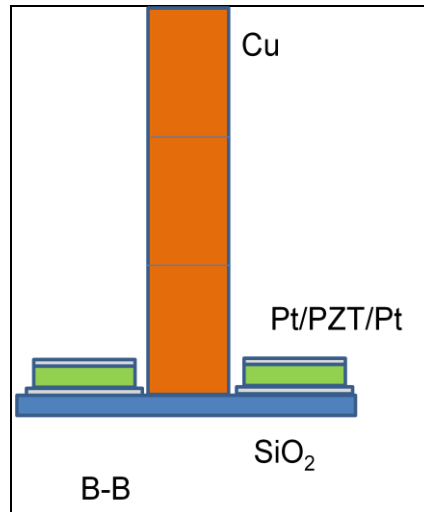
Figure 13. Cross section of s high aspect ratio Cu beam
next to the thin-film PZT sensing beam.
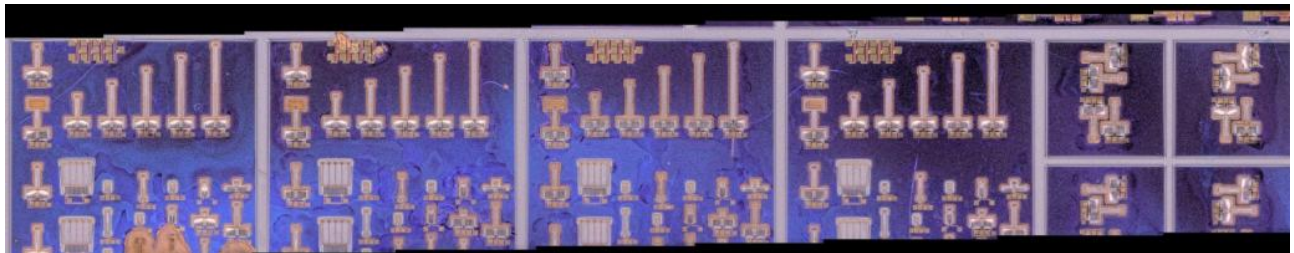
Figure 14. Micrograph of some of the designs in haltere study. Each die had a progressively thicker Cu layer by adding or omitting each respective Cu layer. The image shows five dies. In the fourth die from the left, the Cu thicknesses, haltere length, haltere width, and haltere mass were systematically changed to examine the optimum performance. Arrayed haltere were fabricated in the first four dies as well to measure the coupled response. In the fifth die from the left, haltere designs that are paired/coupled and are capable of detecting all three axes of angular rate are shown.

Thin-film-based versions include the use of PZT actuators at the base of the structure and anchor attachment to enable resonant actuation. PZT sensing sections are located on the sides of a high aspect ratio cantilever section that convert Coriolis force generated strain in the film to a voltage (see figure 5). Electroplated metal, Cu in this case, is used to fabricate high aspect ratio features on the cantilever section. The out-of-plane dimension was thickened to reduce the sensitivity of the PZT sensor to drive motion. Figure 15 shows an SEM of a single haltere. The thick gray lines indicated by the arrow in the left-hand image are the PZT drive actuators that cause the haltere to oscillate in and out of the plane of the image. The thin gray lines along the base of the cantilever indicated by the arrow in the right hand image are the PZT sensors. The large gray rectangles at the top of the left hand image are the contact pads. Two are for driving the actuators, and two are for sensing the perpendicular forces.
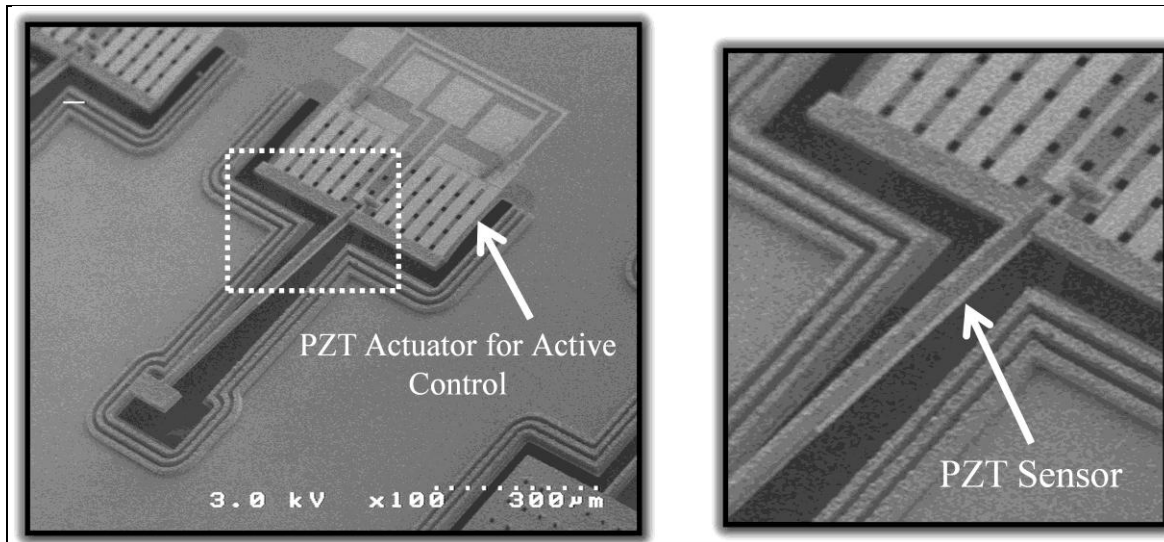
Figure 15. SEM of a PZT-based MEMS haltere with PZT actuators to enable resonant drive and PZT sensors along the cantilever section to detect the strains generated by the Coriolis force acting upon the vibrating proof mass.

3.6 Characterization

Fabricated halteres were characterized to correlate the performance to the simulations, determine optimum properties, and improve the design. A series of characterizations that included materials characterization, in-situ dynamic bend tests, and dynamic device testing were conducted. Additionally, static electrical characterizations were conducted to ensure that electrical connectivity to all portions of the device was within established bounds and that there were no shorts. Materials characterization using the Field Emission Scanning Electron Microscope (FESEM)-FIB at the Weapons and Materials Research Directorate (WMRD) was conducted to examine the grain structure of the complex heterostructures, in both plan view and cross-sectional view. Dynamic bend tests were conducted in the FESEM-FIB to specifically measure the elastic modulus and strength for the complex heterostructures. Finally, dynamic testing was undertaken on the wafer to measure the degree of motion generated by actuating the haltere. In a follow-on investigation, dynamic three-axis angular rates will be measured for a packaged device system.

3.7 Materials Characterization

In a complex heterostructure, it is fundamentally necessary to determine the post-fabrication materials and heterostructure properties. In the initial simulations, when the devices were designed, often idealized material properties would be used, when exact properties were unavailable. To develop a better physical understanding of the overall heterostructure and device performance, a number of tests were conducted.

A series of SEM images were taken of fabricated devices. Figure 16 shows low and high magnification SEM images of an array of haltere fabricated in the ALC cleanroom.

Considerable surface roughness is evident from the high magnification views and the amplitude of surface roughness may exceed 1–2 μm locally. Figure 16 shows FIB-SEM examinations of the respective layer thicknesses of a haltere. Local FIB machining was used to slice through the full thickness of a part. This cross section was imaged both with FIB channeling images and with the SEM. For this particular haltere, the approximate layer thicknesses were as follows: Cu ~6 μm, Top platinum (Pt) ~1 μm, PZT ~0.5 μm, Bottom Pt ~0.2 μm, and SiO_2 ~0.5 μm. Ion channeling images were used to reveal the grain structures in the cross-sections. As shown in figure 17, individual crystallites in the Cu and Pt layers are comparable in images show that individual Cu grains can be comparable in size to the thickness of the layer.
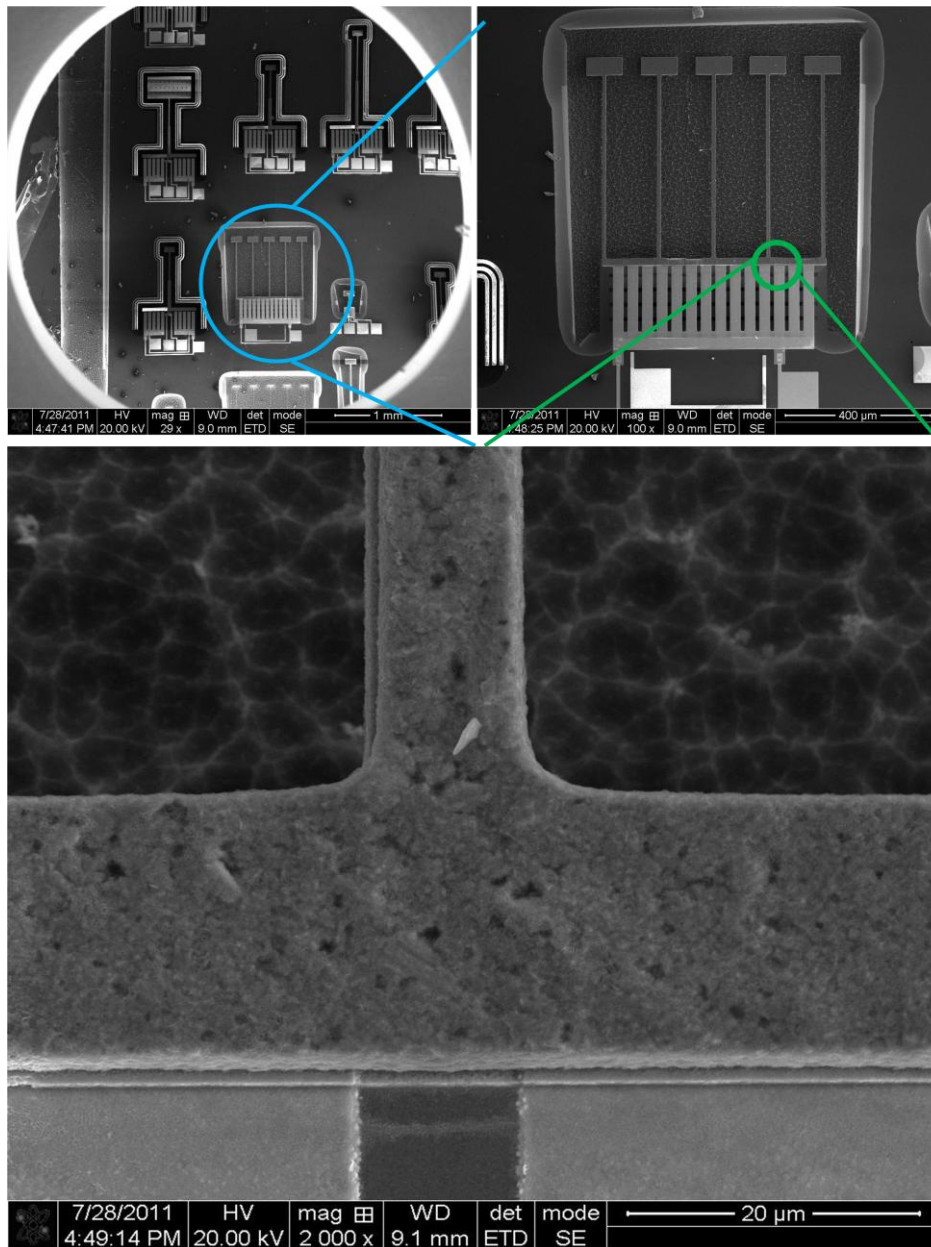
Figure 16. FESEM of the top of an array of haltere.
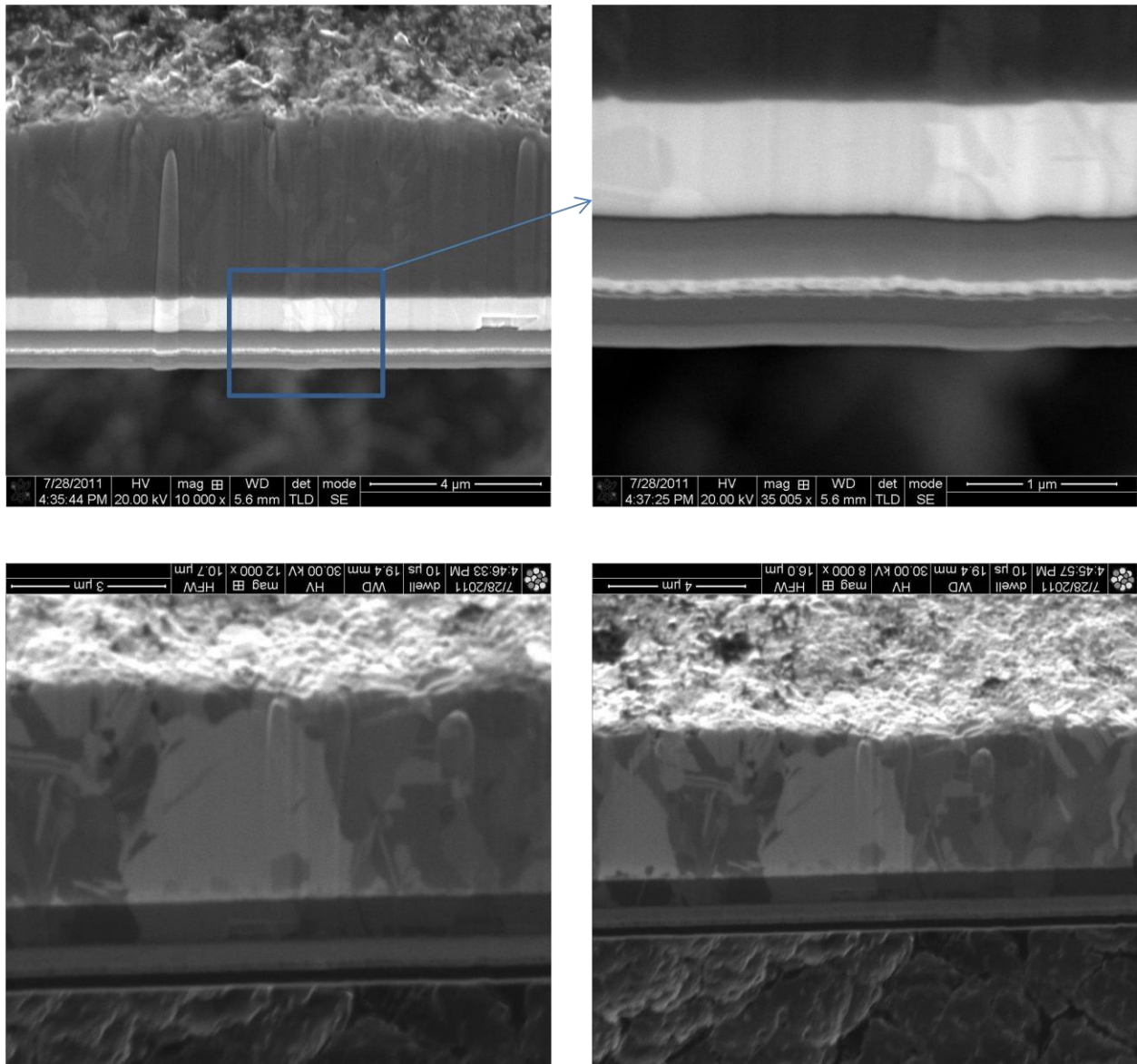
Figure 17. The respective layer thicknesses of the haltere were measured from a FIB machined cross section that was imaged with an SEM. For this particular region, the Cu thickness is roughly 6 μm in depth and the top Pt thickness was 1.0 μm. FIB channeling images show that individual Cu grains can be comparable in size to the thickness of the layer.

3.8 In-situ Dynamic Bend Testing

In order to precisely measure the force response of the fabricated halteres, a series of bend tests were completed in the FESEM-FIB with a load cell. A schematic in-situ SEM test stage and an example of the geometry for a quasi-static (typical in-plane) bend test is shown in figure 18. These tests were used to characterize the quasi-static elastic response for corresponding to the Coriolis force sensing mode shape (in-plane motion and relative strain along the sides of the high aspect ratio beam due to the sideways motion see figure 10). During initial tests, static loads were used to displace one end of the beam. For the mechanical test shown in figure 19, a static

load of 1–2 mN allowed displacement of the mass to deflections of ~125 μm. This load is comparable to the resolution of the load cell and is therefore not sufficient to characterize the load-displacement response of these structures.
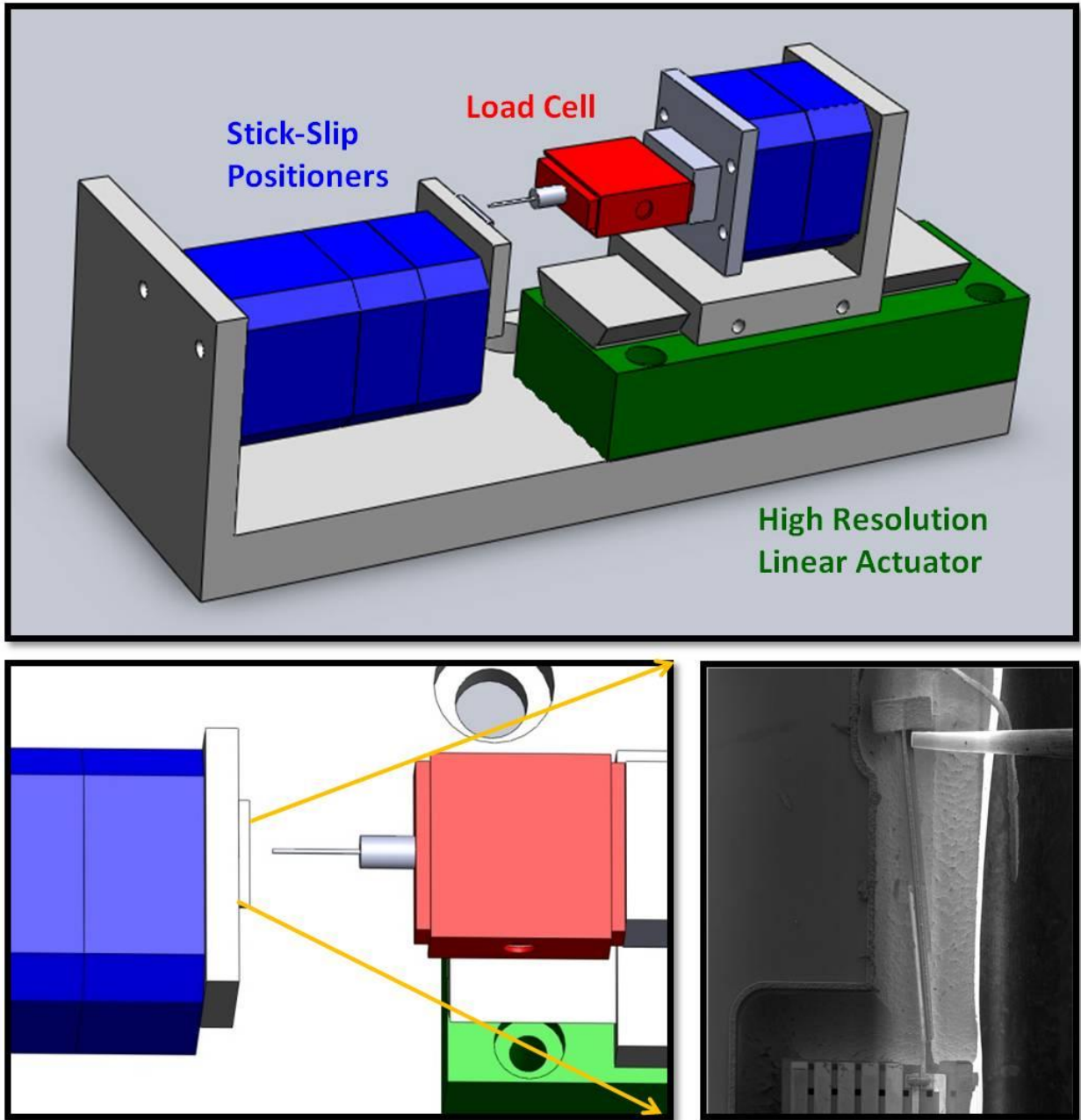
Figure 18. A schematic of the *in-situ* SEM mechanical test stage is shown. In the top image, the "stick-slip actuators" (in blue) allow manipulation of specimens over a ~5 mm range in *x, y* and *z* with a resolution approaching ~100 nm. Loads are applied using a high resolution linear actuator (shown in green) and are measured with a miniaturized S-beam load cell (in red). Loads are applied directly to the structure with a FIB machined tungsten needle (shown on the bottom right).
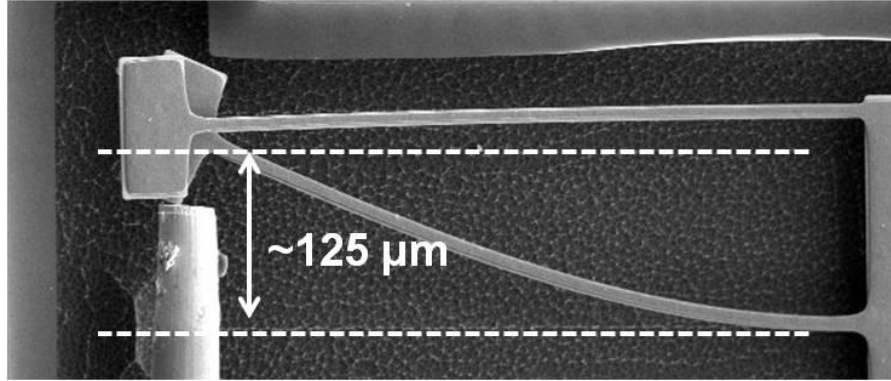
Figure 19. A series of FE-SEM images overlaid showing the dynamic bending of the cantelever as a 0.2 mN force was applied to the tip.

In future work, this in-situ mechanical test stage could be redesigned to incorporate a high resolution load cell or sensing probe. We have indentified load sensing probe capable of resolving forces of ~5 nN and range of 10 mN. This load resolution is offers a ~40 times improvement over the current system and is more appropriate for the load regime required for these highly compliant structures.

3.9   Dynamic Device Testing

Once static electric characterization was completed and in-situ bend tests were done, a series of dynamic tests were undertaken to examine the device properties. Initial dynamic testing of the devices shows excellent performance in terms of frequency and displacement of the end mass. Devices resonant at excellent displacements at 1 to 5 V drive inputs. Higher displacement translates to a higher sensitivity as higher peak velocity of the mass leads to a higher Coriolis force when it experiences the same external angular rate. For example, testing of the PZT/Cu MEMS haltere has demonstrated devices vibrating at 588 Hz with tip displacements of 213 μm for a 500-μm-long haltere beam. A haltere being actively actuated is shown in figure 20. The image to the left is the haltere without any applied electrical field, while the image on the right is the same haltere under and applied field of 6 V.
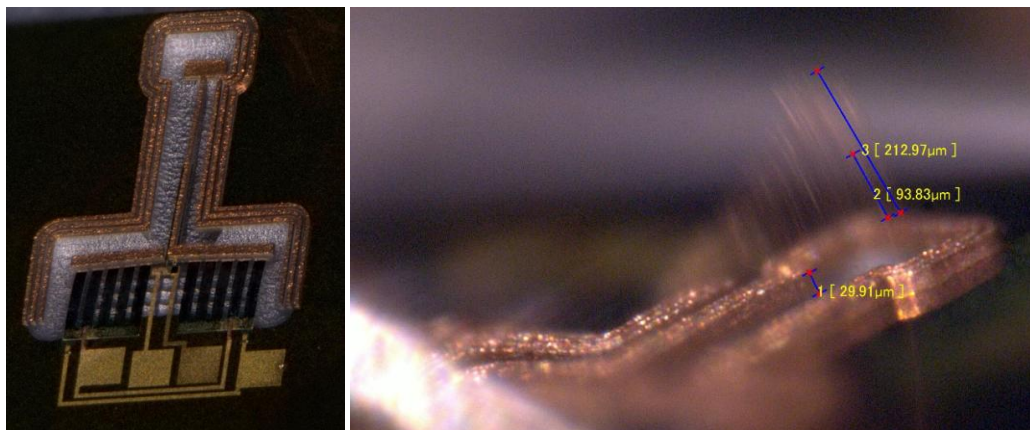
Figure 20. (a) Micrograph of released haltere and (b) micrograph of haltere at resonance with 6-V input and 213 μm of Cu mass displacement.

Characterization of output signal to rotational rate is pending and was started in December 2011. The individual dies were placed in 24 dual inline package (DIP) Kovar, packaged, and wirebonded. A circuit that will buffer, amplify, and convert the signal from analog to digital has been designed and fabricated. Mechanical rotation of this circuit board will be performed at Aberdeen Proving Ground (APG) in collaboration with Vehicle Technology Directorate (VTD) on a custom designed three-axis gimbaled rate table (figure 21). The table meets all the requirements needed to characterize haltere on a single axis like any standard rate table, but was also chosen for the potential to characterize a system of haltere in all three rotation axes. Results of the pending test will validate the models and be used to iterate the design.
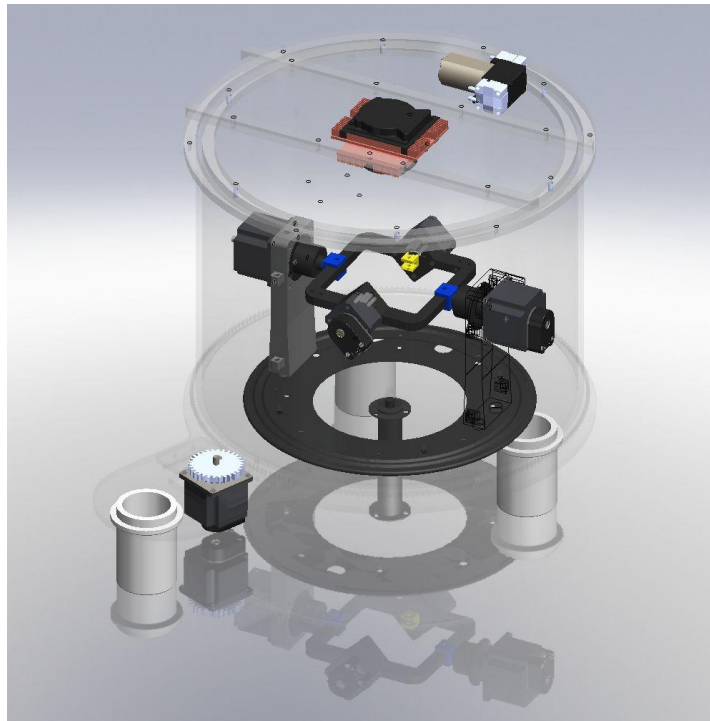
Figure 21. The three-axis rate table, designed and fabricated by VTD, to be
used to charaterize the PiezoMEMS haltere.

4.   Conclusions

MEMS-scale haltere sensors were successfully designed and fabricated with a control scheme that enables simple, straightforward decoupling of the signals. Results were presented in four principal areas that contributed to this success:

1. Passive mechanical logic was designed to facilitate the decoupling of the forces acting on the sensor.

2. A control scheme was developed that efficiently and accurately decouples the three component parts from the haltere sensors.

3. Individual, coupled, and arrayed halteres were fabricated in the MEMS foundry at ARL-ALC.

4. The materials, composite, and dynamic testing has been initiated and is underway on the completed sensors.

A series of static electrical tests and dynamic device tests were conducted, in addition to in-situ bend tests, to validate the initial simulation results. The simulation and experimental results, taken as a whole, indicate that the area of the PZT designated for sensing will be inherently sensitive to the Coriolis forces caused by changes in angular rate.

The successful fabrication of a micro-ARS represents a substantial breakthrough. This is an enabling technology for a number of Army applications, including MAVs. There are already a number of MAV designers that are actively collaborating with us to facilitate the transition of this sensor system into a MAV avionics package.

At time of submission (December 2011), the sensor system in development within this DRI is the world's smallest three-axis ARS.

5. References

Alexander, R. M. Antennae as Gyroscopes. *Science* **2007**, *315* (5813), 771–772. Retrieved from http://www.sciencemag.org/content/315/5813/771.full.

Alexander, R. M. Antennae as Gyroscopes. *Science* **2007**, *315* (5813), 771–772. Retrieved from http://www.sciencemag.org/content/315/5813/771.full.

Bedair, S. S.; Pulskamp, J. S.; Meyer, C. D. ARL DRI Report, FY11-SED-026, In Press. 2012.

Bender, J. A.; Frye, M. A. Invertebrate Solutions for Sensing Gravity. *Current Biology* **2009**, *19* 186–190.

Chan, W. P.; Prete, F.; Dickenson, M. H. Visual Input to the Efferent Control System of a Fly's "Gyroscope". *Science* **1998**, 289–292.

Chen, Y.; Wicaksono, D.H.B.; Pakula, L.; Rajaraman, V.; French, P. J. Modeling, Design and Fabrication of A Bio-inspired MEMS Vibratory Gyroscope. *in Proceedings of Semiconductor Advances in for Future Electronics (SAFE) 2007*, pp. 572–576, Veldhoven, The Netherlands, 29–30 November 2007.

Dragonfly Woman, 2010. http://thedragonflywoman.com/2010/04/21/giantskeeter/crane-fly-halteres/ (accessed 2011).

Frankel G.; Pringle, J.W.S. Halteres of Flies as Gyroscopic Organs of Equilibrium. *Nature* **1938**, *141*, 919–921.

Hengstenberg, R. Mechanosensory Control of Compensatory Head Roll During Flight in the Blowfly Calliphoraerythrocephala Meig. *Journal of Comparative Physiology A* **1988**, *163*, 151–165.

Jordan, K.; Bueno, J.; Reid, C.; Schneider, K.; Bedair, S. S.; Smith, G.; Nothwang, W. D.; Wickenden, A. E. *A Systematic Study of the Factors Influencing Coriolis Force Sensitivity on a Bio-inspired Haltere*; U.S. Army Research Laboratory: Adelphi, MD, in preparation a.

Jordan, K.; Reid, C.; Schneider, K.; Bedair, S. S.; Smith, G.; Nothwang, W. D.; Wickenden, A. E. *A Control Circuit Design to Measure the Coriolis Force Sensitivity on a Bio-inspired Haltere*; U.S. Army Research Laboratory: Adelphi, MD, in preparation b.

Lambert Smiths Insecta: South African Insects and Macro-photography, 2009. http://www.insecta.co.za/index.php?option=com_content&view=article&id=58&Itemid=66 (accessed 2011).

Motamed, M.; Yan, J. A Review of Biological, Biomimetic and Miniature Force Sensing for Microflight. *International Conference on Intelligent Robots and Systems* (pp. 3939–3946). IEEE IROS. 2005.

Nalbach, G.; Hengstenberg, R. The Haltere of the Blow Fly Callifera. *Journal of Comparative Physiology A: Neuroethology, Sensory, Neural, and Behavioral Physiology* **1994**, *175* (6), 695–708.

Pfieffer, M. http://www.fva-bw.de/forschung/bu/bodenschluessel/img/orginf_halteren.jpg (accessed 2011).

Pringle, J. The Gyroscopic Mechanism of the Halteres of Diptera. *Philosophical Transactions Biological Sciences* **1948**, 347–385.

Proie, R. M.; Polcawich, R. G.; Pulskamp, J. S.; Ivanov, T.; Zaghloul, M. Nano-electromechanical Storage Element for a Low Power Complimentary Logic Architecture Using PZT Relays. *Solid-State Sensors, Actuators and Microsystems Conference (TRANSDUCERS) 16th International Conference*, 5–9 June 2011, Beijing, 840–843, 2011.

Sherman, A.; Dickinson, M. A Comparison of Visual and Haltere-mediated Equilibrium Reflexes in the Fruit Fly *Drosophila Melanogaster.* *J Exp Biol* **January 15, 2003**, *206*, 295–302.

Smith, G. L.; Bedair, S. S.; Schuster, B. E.; Nothwang W. D. Haltere Based Angular Rate Sensors. *Journal of SPIE*, Invited, in press, 2012.

Smith, G. L.; Bedair, S. S.; Schuster, B. E.; Nothwang W. D. Haltere Based Angular Rate Sensors. *SPIE-DSS*, Invited, Baltimore, MD, 2012.

Smith, G. L.; Pulskamp, J. S.; Sanchez, L. M.; Potrepka, D. M.; Proie, R. M.; Ivanov, T. G.; Rudy, R. Q.; Nothwang, W. D.; Bedair, S. S.; Meyer, C. D.; Polcawich, R. G. PZT-based Piezoelectric MEMS Technology. *Journal of the American Ceramic Society-Invited*, In Press. 2011.

Thompson, R. A. *Haltere Mediated Flight Stabilization in Diptera: Rate Decoupling, Sensory Encoding, and Control Realization*; Gainesville: University of Florida, 2009.

Thompson, R. A.; Wehling, M. F.; Evers, J. H.; Dixon, W. E. Body Rate Decoupling Using Haltere Mid-stroke Measurements for Inertial Flight Stabilization in Diptera. *Journal of Comparative Physiology A* **2009**, *195,* 99–112.

Wu, W. C.; Schenato, L.; Wood, R. J.; Fearing, R. S. Biomimetic Sensor Suite for Flight Control of a Micromechanical Flying Insect: Design and Experimental Results. *IEEE Int. Conf. on Robotics and Automation*, Taipei, Taiwan, May 2003.

6. Transitions

This work has already resulted in two invited publications (Smith et al., 2011; Smith et al., 2012) and one invited presentation (Smith et al., 2012). Two technical reports have resulted from this work and are in preparation (Jordan et al., in preparation a,b).

Additionally, work has begun to integrate haltere-based ARS into the avionics of Professor Rob Wood's Robo-fly at Harvard and Professor Sean Humbert's mini-Quad at the University of Maryland.

Work is continuing on this effort in the PiezoMEMS and the Nano and Micro Sensors Teams' mission programs.

Future Work

Initial data from these tests were also presented. These data will be used to optimize the sensor performance and establish baseline material property values for use in future ANSYS simulations. The load resolution of the current in-situ FESEM-FIB-based test system was not sufficient to characterize the elastic response of the halteres. We have identified a load sensing probe capable of resolving loads as small as ~5 nN over a range of 10 mN. The load range and resolution are more appropriate for the load regime required to deflect the haltere structures. Complete testing of this sensor system including three-axis angular rate and complete materials characterization is underway and will be reported over the following year.

List of Symbols, Abbreviations, and Acronyms

3-D   three-dimensional

A-D   analog-to-digital

ALC   Adelphi Laboratory Center

APG   Aberdeen Proving Ground

ARL   U.S. Army Research Laboratory

ARS   angular rate sensor

Au   gold

CMOS   complementary metal-oxide semiconductor

Cu   copper

DIP   dual inline package

DRI   Directors Research Initiative

FESEM   Field Emission Scanning Electron Microscope

FIB   focused ion beam

IMUs   inertial measurement units

MAVs   Micro Air Vehicles

MEMS   micro electro-mechanical systems

PiezoMEMS   piezoelectric MEMS

Pt   platinum

PZT   lead zirconate titanate

SEM   scanning electron microscope

SEMASC   Specialty Electronic Materials and Sensors Cleanroom

SiO_2 silicon dioxide

SWaP   size, weight and power

VTD   Vehicle Technology Directorate

WMRD   Weapons and Materials Research Directorate

No of.
Copies   Organization

10 HCS   US ARMY RSRCH LAB
         ATTN RDRL-SER-L
         GABRIEL SMITH
         SARAH BEDAIR
         BRETT PIEKARSKI
         VISHNU GANESAN
         KESSHI JORDAN
         CORDELL REID
         KATHRYN SCHNEIDER
         CHRIS MEYER
         ALMA WICKENDEN
         WILLIAM NOTHWANG
         ADELPHI MD 20783-1197

1 HCS   US ARMY RSRCH LAB
         ATTN RDRL-WML-H
         BRIAN SCHUSTER
         B434 MULBERRY RD.
         ABERDEEN PROVING GROUND MD 21005

TOTAL: 11 (11 HCS)